



Published in final edited form as:

*Traffic*. 2014 December ; 15(12): 1330–1343. doi:10.1111/tra.12211.

## Quantitative Analysis of Membrane Trafficking in Regulation of Cdc42 Polarity

Leah J. Watson, Guendalina Rossi, and Patrick Brennwald\*

Department of Cell Biology & Physiology, University of North Carolina at Chapel Hill, Chapel Hill, NC 27599 USA

### Abstract

Vesicle delivery of Cdc42 has been proposed as an important mechanism for generating and maintaining Cdc42 polarity at the plasma membrane. This mechanism requires the density of Cdc42 on secretory vesicles to be equal to or higher than the plasma membrane polarity cap. Using a novel method to estimate Cdc42 levels on post-Golgi secretory vesicles in intact yeast cells, we: 1) determined that endocytosis plays an important role in Cdc42's association with secretory vesicles 2) found that a GFP-tag placed on the N-terminus of Cdc42 negatively impacts this vesicle association and 3) quantified the surface densities of Cdc42 on post-Golgi vesicles which revealed that the vesicle density of Cdc42 is three times more dilute than that at the polarity cap. This work suggests that the immediate consequence of secretory vesicle fusion with the plasma membrane polarity cap is to dilute the local Cdc42 surface density. This provides strong support for the model in which vesicle trafficking acts to negatively regulate Cdc42 polarity on the cell surface while also providing a means to recycle Cdc42 between the cell surface and internal membrane locations.

### Introduction

Growth along a defined axis is important for many biological processes. The subcellular localizations of key regulators and effectors of polarity are intricately linked with their control of the establishment and maintenance of the polarized axis [1–4]. In budding yeast, the switch from isotropic to asymmetric growth is preceded by the accumulation of activated (GTP)-Cdc42—a conserved Rho GTPase—at the presumptive bud site [5, 6]. The Cdc42 polarity cap is required to orient the actin and secretory pathways toward the nascent bud site and Cdc42 polarization is necessary and sufficient for determining the site of bud emergence [2, 4].

Generation and maintenance of robust Cdc42 polarity promotes membrane expansion during bud formation. Studies reveal that Cdc42 is dynamically maintained at the polarity cap through its continuous cycling between the polarity cap and internal pools [7–9]. Two major mechanisms for recycling Cdc42 have been described. In one mechanism, GDP-Cdc42 is rapidly recycled by the sole yeast Rho GDP dissociation inhibitor, Rdi1. In the other

\*Correspondence to pjbrennw@med.unc.edu.

The authors have no conflict of interest to declare.

proposed mechanism, actomyosin-based exocytic delivery of Cdc42 is coupled to a slower endocytic retrieval pathway. Both mechanisms presumably circumvent the lateral membrane diffusion of Cdc42 by coupling Cdc42 delivery to a localized GEF-mediated positive feedback system [8, 10–13]. Although endogenous Cdc42 has been shown to associate with secretory vesicles [11, 14, 15], a recent report using mathematical modeling challenges a possible role for membrane trafficking in polarizing Cdc42 [16]. Common methods for estimating the vesicle-bound pool of Cdc42 either subject cells to lysis conditions or require fluorescently tagged protein—both of which may impede direct quantitative assessment of the membrane association of the native protein.

In this study, we make use of a novel assay to quantitatively assess the contribution of the recycling pathways to the polarity of endogenous Cdc42 and obtain estimations of the relative and absolute concentrations of Cdc42 on post-Golgi vesicles and the plasma membrane polarity cap. While our results implicate endocytic and exocytic trafficking in recycling of Cdc42, they also demonstrate that the density of Cdc42 protein on exocytic vesicles is significantly lower than at the plasma membrane polarity cap. We discuss the implications of these findings on current models for Cdc42 polarization.

## Results

### A quantitative assay for Cdc42-vesicle association

Previous work utilizing thin section electron microscopy demonstrated that *GAL*-induced overexpression of either of two Sec4 effector proteins, Sec15 or Sro7, results in the formation of a large, homogeneous cluster of tightly, compacted 80–100 nm post-Golgi secretory vesicles within the cytosol [17–19]. We made use of this observation to establish a novel *in vivo* assay for quantitatively examining the association of Cdc42 with post-Golgi vesicles as a complement to earlier studies that used subcellular fractionation and other biochemical methods for vesicle purification [11, 14, 15]. As observed previously, *GAL*-induced overexpression of either Sec15 or Sro7 results in a marked change in the localization of Sec4 from sites of polarized growth to a large cytoplasmic patch within the cell which corresponds to a cluster of post-Golgi vesicles observed by thin section electron microscopy [17–19] (Figure 1A). Consistent with results from biochemical studies, double-labeled immunofluorescence staining with antibodies directed at Cdc42 and Sec4 revealed a striking re-localization of Cdc42 from the bud-tip to the Sec4-positive vesicle clusters in response to the Sec15 or Sro7 induction (Figure 1A). In both Sec15- and Sro7-induced cells we find that all the cytoplasmic clusters that are positive for Cdc42 are also positive for Sec4 and that greater than 70% of Sec4-positive clusters were positive for Cdc42 (Figure 1B). This is similar to the level of co-localization observed at the plasma membrane polarity cap in uninduced cells (*GAL*-vector, Figure 1B).

As a first step in the quantification of Cdc42 levels found on specific membrane compartments, we measured the ratio of Cdc42 fluorescence associated with Sec4-positive vesicle clusters or the plasma membrane polarity cap to an equivalent-sized region in the cytoplasm. The relative Cdc42 fluorescence associated with vesicle clusters was greater than (*GAL-SEC15*) or similar to (*GAL-SRO7*) that seen for the polarity cap observed in control (*GAL*-vector) cells (Figure 1C). Therefore, Cdc42 appears to be present on post-Golgi

vesicles at levels comparable to the plasma membrane polarity cap. However to properly address the question posed by the trafficking model concerning the relative concentration of Cdc42 on vesicles compared to the plasma membrane polarity cap, it was important to also take into careful consideration the membrane surface areas contributing to each of these fluorescence measurements (see section on quantification of Cdc42 densities below).

### Endocytosis is required for Cdc42 post-Golgi vesicle association

Recycling of Cdc42 to and from the plasma membrane polarity cap is thought to be critical to its ability to act in cell polarization. Two mechanisms for Cdc42 recycling have been proposed. One mechanism involves the Rho GDI protein which selectively extracts the GDP-bound form of geranylgeranylated Cdc42 from the plasma membrane by providing a pocket for the hydrophobic prenyl group—similar to the role for Rab GDI in Rab GTPase recycling [20]. The second mechanism involves endocytic recycling of Cdc42 from the plasma membrane in a pathway that may function in parallel to its recycling by Rho GDI [8, 9, 21]. We made use of the vesicle clustering assay described above to examine the requirement of GDI or endocytosis in the association of Cdc42 with post-Golgi vesicles. To examine the endocytic requirement, we disrupted endocytosis using a deletion in *END4* (also known as *SLA2*) which regulates the interaction between endocytic vesicles and the actin cytoskeleton during vesicle internalization [22]. As expected (Figure 2A), Cdc42 localization at the plasma membrane polarity cap is stable in cells lacking *RDII* or *END4* [8, 9, 11, 23]. However, induction of vesicle clusters in an *end4* background resulted in >60% reduction in the relative concentration of Cdc42 associated with vesicle clusters in *Sro7*- or *Sec15*-overexpressing cells (Figure 2B, C, E and F). Examination of the penetrance of this phenotype demonstrated that greater than 70% of cells exhibited a dramatic reduction (by more than 50%) in the levels of Cdc42 present in the *Sec4*-positive vesicle clusters (Figure 2D, G). Disruption of *RDII* function did not negatively affect cluster association of Cdc42 in either *Sro7*- or *Sec15*-overexpressing cells (Figure 2B through G). Indeed, *rdi1* cells had increased levels of Cdc42 associated with vesicles—which is consistent with the documented depletion of cytosolic Cdc42 in *rdi1* cells [9, 11, 23]. Therefore, while endocytosis is important for Cdc42 association with post-Golgi vesicles, Rho GDI is completely dispensable for this association.

We next examined the association of Cdc42 with vesicle clusters in mutants known to have defects at distinct points in endocytic trafficking from the plasma membrane to endosomes and the Trans Golgi Network (TGN). *Sla1*, like *End4*, functions at the plasma membrane during endocytic vesicle formation, while *Tlg2* and *Pep12* are important for transport between the early endosome to the TGN and between the late endosome (or PreVacuolar Compartment) and the TGN, respectively [24]. We found that defects in any of these gene products results in a significant and highly penetrant defect in Cdc42 association with vesicle clusters, suggesting that Cdc42 recycling onto post-Golgi vesicles is likely to involve trafficking through multiple endocytic compartments (Figure 3A, B).

Cdc42 has previously been shown to associate with post-Golgi vesicles that accumulate in response to a *sec6-4* mutation when analyzed by differential centrifugation [14]. To examine the role of endocytic and GDI-mediated recycling on the association of Cdc42 with post-

Golgi vesicles by differential centrifugation, we constructed double mutants of *rdi1* or several endocytic mutants with *sec6-4*. In response to a *sec6-4* mutation, cells shifted to 37°C accumulate post-Golgi secretory vesicles which pellet selectively at 100,000 × g (P100). This effect is observed by a large increase in the levels of Sec4 in the P100 fraction in a *sec6-4* strain compared to control wild-type cells. Consistent with previous reports [11, 14], an increase in Cdc42 association with the P100 fraction also occurs in response to the secretory vesicle accumulation (Figure 3C, D). We also observed that when *rdi1*, *sec6-4* cells were examined, elevated levels of Cdc42 were maintained in the P100 fraction. In contrast, the P100 fraction of *pep12*, *sec6-4* mutants—despite having normal accumulation of Sec4—was depleted of Cdc42 compared to *sec6-4* cells (Figure 3C, D). The accumulation of secretory vesicles in the *end4*, *sec6-4* double mutant was problematic and, unfortunately, this mutant could not be utilized for analysis by fractionation. Nonetheless, the results of fractionation clearly confirm both a role for endocytic recycling and the lack of a requirement for GDI function in the association of Cdc42 with exocytic vesicles.

### GFP-Cdc42 shows impaired association with post-Golgi vesicles

Previous work from our lab has demonstrated an important role for the N-terminus of Rho family GTPases in determining their patterns of subcellular localization [3]. Perhaps not surprisingly, several groups have demonstrated significant growth defects associated with N-terminal GFP-tagged forms of Cdc42 expressed as the sole source of Cdc42 in the cell [12, 25, 26]. Since the work described above relied exclusively on untagged Cdc42 expressed from its endogenous chromosomal locus, we examined the effect of a GFP-tagged form of Cdc42 on its association with post-Golgi vesicles in our vesicle clustering assay. We generated strains containing *GAL-SEC15* with either GFP-tagged or untagged *CDC42* expressed behind their native promoter on a *CEN/LEU2* plasmid as the sole source of *CDC42*. Expression from the *CEN* plasmids results in a slight, but equivalent, increase in overall Cdc42 levels (Figure S1D). Although both constructs show normal growth and polarization at 25°C (Figure 4A, B), the GFP-tagged form of Cdc42 resulted in lethality at 37°C as previously reported (Figure S1A, 4D) [12, 25, 26]. When induced with galactose, we saw the expected staining of untagged Cdc42 on the large cytoplasmic puncta co-stained by Sec4. However, the strain containing the GFP-tagged form of Cdc42 demonstrated very weak staining of these puncta that was only slightly above the levels of the surrounding cytoplasm (Figure 4A, C). These data indicate that the presence of a GFP tag on the N-terminus of Cdc42 results in a dramatic loss of post-Golgi vesicle association in this assay.

As mentioned above, Slaughter *et al.* [9] have proposed two parallel mechanisms for recycling of Cdc42: 1) Rdi1-mediated membrane extraction and re-delivery through the cytosol and 2) endocytic uptake and redelivery on exocytic vesicles. A clear prediction of this model is that loss of the sole Rho GDI in yeast should demonstrate synthetic growth defects when combined with a form of Cdc42, in this case GFP-Cdc42, which disrupts its association with exocytic vesicles. We therefore utilized a plasmid shuffle assay to examine the effect of an *rdi1* on the ability of GFP-Cdc42 to function as the sole source of Cdc42 in the cell. Previous reports have demonstrated that GFP-Cdc42 is unable to support growth at high temperatures [12, 25, 26]. We find that the temperature-sensitive nature of GFP-Cdc42 is accentuated by the presence of *rdi1*. In particular, the synthetic effect of the GFP tag and

loss of Rho GDI is most apparent at 34.5°C, a temperature at which GFP-Cdc42 is viable with *RDII* (Figure 4D). While this synthetic sickness at 34.5°C is consistent with the parallel functions for endocytosis and *RDII*, the viability at ambient temperatures and the sustained polarized localization also suggests that there may be a third mechanism for recycling Cdc42 that is independent of both *RDII* and endocytic/exocytic recycling.

### Quantification of Cdc42 density on vesicles and the plasma membrane polarity cap

While previous studies using subcellular fractionation as well as the immunofluorescence studies described above have established that Cdc42 is associated with post-Golgi vesicles in significant amounts, the precise density of Cdc42 molecules on the surface of these vesicles has not been determined. The vesicle clustering procedure described above presented a unique opportunity to address this question *in vivo*, without the numerous difficulties—such as degradation and membrane disassociation—that are often associated with biochemical fractionation. Therefore, we set out to determine the absolute density of Cdc42 molecules on both post-Golgi vesicles (within the clusters) as well as at the plasma membrane polarity cap. This required having reliable estimates of: 1) the total number of molecules of Cdc42 in the cell 2) the membrane surface area associated with the vesicle clusters or the plasma membrane polarity cap and 3) the fractional amount of Cdc42 associated with each of these two regions.

Surprisingly, we were unable to find a direct estimate of Cdc42 copies per cell in whole proteome-tagging studies [27] or other published work. We therefore generated our own estimate by a ratio-metric comparison of GFP fluorescence of a yeast strain containing GFP-Cdc42 on a *CEN* plasmid with a reference strain containing a GFP-tagged form of the kinetochore protein Cse4—of which the copy number per sister kinetochore cluster is well established [28–30]. To compare the relative fluorescence levels of GFP-Cdc42 in the total cell and Cse4-GFP in the sister kinetochore clusters, the two strains were mixed and imaged by fluorescence microscopy (Figure 5A). With each sister kinetochore containing 80 copies of Cse4, the resulting comparison yielded an estimate of roughly 27,400 copies of GFP-Cdc42 per cell. We then compared the amount of plasmid-derived GFP-Cdc42 to that of endogenous Cdc42 in wild type cells by quantitative Western blot analysis (Figure 5B). From this analysis we estimate that wild type cells contain approximately 6,800 copies of Cdc42 per cell.

Since the growth conditions for the vesicle clustering assays differed from the above conditions, we compared the effects of carbon source and vesicle clustering on Cdc42 amounts per cell. While we found there was little effect of carbon source (glucose vs. raffinose; data not shown) on the levels of Cdc42, there was a significant (>50%) increase in Cdc42 amounts in strains when vesicle clusters were induced (Figure 5C). This is presumably due to the enlargement of cells and the inhibition of cell division during vesicle cluster formation. Based on this comparison, we estimate approximately 10,400 copies of Cdc42 per cell following the 8 hour galactose induction of *Sec15*—identical to the conditions used for fluorescence imaging.

We next utilized morphometric analysis of thin-section electron micrographs to determine the packing density of post-Golgi vesicles associated with *GAL-SEC15* and *GAL-SRO7*

induced vesicle clusters used for fluorescence imaging (Figure 5E, F). This analysis demonstrated that the vesicle clusters contained approximately  $35.5 \pm 3.9$  post-Golgi vesicles (90nm average diameter) per square micron for each thin section. Thus, the 0.718 micron diameter regions of interest (ROI) used for fluorescence imaging (0.2 $\mu$ m thick optical sections) of clusters corresponded to approximately 71 vesicles or a total vesicle membrane surface area of 0.723 square microns per ROI. Fluorescence microscopy was used to determine the fractional amount of Cdc42 (% of total) associated with each ROI. Considering the total copy number of Cdc42 in the cell, our assessment yielded ~187 copies of Cdc42 in the vesicle cluster ROI. This corresponds to approximately 6.5 copies of Cdc42 per vesicle or a density of ~260 copies of Cdc42 per square micron of vesicle surface (Figure 5E, G).

To assess Cdc42 surface density at the plasma membrane polarity cap, we imaged cells using the same growth conditions as above but without Sec15 induction (*GAL*-vector). This imaging revealed a fractional fluorescence of approximately 93 copies of Cdc42 per ROI. Since thin section electron micrographs of small budded yeast show an average of  $1.3 \pm 0.23$  secretory vesicle in close proximity to the bud tip per section (per bud) or approximately 2.6 vesicles per 0.2 micron optical section, it was important to account for this contribution in our estimates. To accomplish this we subtracted the contribution of the 2.6 docked vesicles (~17 copies of Cdc42) from the total Cdc42 present in the ROI (93 copies) and divided the remaining amount (76 copies) by the plasma membrane surface area present in the ROI (0.094  $\mu$ m<sup>2</sup>). As shown in Figure 5G, this equates to a plasma membrane cap density of 810 copies of Cdc42 per square micron which is nearly three times the density of Cdc42 on the vesicle membrane (260 copies/ $\mu$ m<sup>2</sup>).

To corroborate our findings described above, we also generated an estimate of the Cdc42 copy number by quantitative immunoblot analysis using an alternative reference standard, Sec1—a protein which the total copies per cell (determined by immunoblot) has previously been determined [27]. We generated a strain in which Sec1-GFP was integrated at the *SEC1* chromosomal locus such that it is expressed behind the native promoter and is the sole source Sec1 in the cell (see materials methods). Whole cell lysates of Sec1-GFP and GFP-Cdc42 expressing cells alongside an isogenic control strain were prepared, loaded by equivalent cell number and analyzed by Western blotting (Figure 5D). We applied the reported total copies of Sec1 (639 copies/cell) to the ratio of total GFP-Cdc42:Sec1-GFP and found the total copies of GFP-Cdc42 to be roughly 21,500. Using this copy number and the aforementioned comparative analyses of native Cdc42 protein levels under various conditions (see Figures 5B, C), we estimate ~5,400 copies of Cdc42 in polarized (uninduced) cells and ~8,200 copies of Cdc42 in cluster-forming (induced) cells. The compilation of the described data using both reference standards is reported in Figure 5G. Similar to our results using the Cse4 standard, we found the plasma membrane cap density of 636 Cdc42 copies per square micron to also be roughly three times the vesicle membrane density (204 copies/ $\mu$ m<sup>2</sup>). Together these data suggest the immediate effect of post-Golgi vesicle fusion with the Cdc42 polarity cap would be to dilute rather than concentrate Cdc42 at the site of fusion. The implications of this surprising finding are discussed below.

## Discussion

Delivery of Cdc42 by vesicle-mediated exocytic transport has been proposed to be an important mechanism by which Cdc42 polarity on the plasma membrane is both generated and maintained [14, 31]. In these models, Cdc42 associated with post-Golgi vesicles is delivered along actin cables to sites of polarized growth. The subsequent fusion of Cdc42-laden vesicles with the plasma membrane at these sites would promote Cdc42 polar cap formation. This would lead to a positive feedback loop by reinforcing the organization of actin cables oriented toward such sites, which in turn would bring more vesicles to this site [2, 14]. Another positive feedback loop could result from Cdc42's direct activation of the Exocyst tethering complex to promote its own polarization by increasing the rates of vesicle docking and fusion at specific sites of the plasma membrane—in a manner that is independent of actin [31, 32]. A critical assumption in both of these models is that the surface density of Cdc42 on post-Golgi vesicles must exceed the surface density at the plasma membrane polarity cap for polarity to be generated and/or maintained [16]. Mathematical modeling studies by Savage *et al.* [33], examined the theoretical effect of exocytic fusion of vesicles depleted of Cdc42 on the plasma membrane polarity cap. In their model such a situation perturbed local polarity in a manner that could be overcome in the presence of an active GDI recycling mechanism. The experimental data presented here demonstrate that such an effect is more than theoretical since the surface density we observe for Cdc42 on post Golgi vesicles is, in fact, roughly 3-fold more dilute than the density of Cdc42 we observe at the plasma membrane polarity cap. This indicates that the immediate effect of exocytic vesicle fusion is to dilute the Cdc42 present at this site on the plasma membrane rather than to concentrate it, which is inconsistent with the actin-mediated positive feedback model [9, 14].

Since both the actin cytoskeleton and the vesicle docking/fusion apparatus are thought to direct traffic to sites on the plasma membrane with the most concentrated Cdc42, the local effect of exocytic transport would be to antagonize or destabilize Cdc42 polarization on the plasma membrane [13, 34]. Local negative regulation may play an important role in building spatial flexibility into this system. This is similar to a model recently proposed by Dyer *et al.* [35] in which dilution of the scaffolding protein Bem1 by vesicle fusion would lead to wandering of the polarity cap. Our data suggest that in addition to dilution of polarity factors such as Bem1, vesicle fusion would result in dilution of Cdc42 itself which would contribute directly to the destabilizing effect of exocytic transport on polarity.

If the immediate effect of exocytic traffic is to antagonize Cdc42 polarity on the plasma membrane, then why is Cdc42 associated with post-Golgi vesicles at all? While the work presented here does not directly address this important question, we can speculate on possible roles for exocytic delivery of Cdc42. First, exocytic delivery may represent a mechanism for recycling Cdc42 that has been removed by endocytosis [8, 9, 21]. Such a delivery system would fit with the notion that trafficking acts as a parallel pathway to the Rho GDI recycling mechanism as proposed by Slaughter *et al.* [9]. All of our data is in complete agreement with such a recycling function for vesicular Cdc42. Another function for this recycling mechanism is that having significant levels of Cdc42 on the vesicles helps

to buffer the negative regulatory effects of exocytic transport on Cdc42 polarity a possibility explored through modeling in the Savage *et al.* study [33].

A recent study examined the apparent surface densities of GFP-Cdc42 within the cell by fluorescence correlative spectroscopy [36]. In this paper, Slaughter *et al.* concluded that the surface density of GFP-Cdc42 on vesicles (49 molecules/ $\mu\text{m}^2$ ) was similar to that on the plasma membrane (46 molecules/ $\mu\text{m}^2$ ). The remarkably low absolute density reported at the polarity cap was particularly surprising given that such a density would involve a polarity cap (0.1 $\mu\text{m}^2$ ) with only 4.3 GFP-Cdc42 molecules out of roughly 12,000 molecules per cell (based on a conservative estimate of the GFP-Cdc42/native Cdc42 expression levels for the GFP-Cdc42 constructs used) or less than 0.04% of the total cellular GFP-Cdc42. In contrast, our estimates of native Cdc42 densities on post-Golgi vesicles are almost 5-fold higher (260 molecules/ $\mu\text{m}^2$  or 6.5 copies per vesicle) than Slaughter *et al.* (2013) and our estimates of densities on the plasma membrane (810 molecules/ $\mu\text{m}^2$ ) are 15-fold higher. For comparison, our results indicate that a polarity cap (0.1 $\mu\text{m}^2$ ) contains 76 molecules of native Cdc42 or roughly 1.1% of the total cellular Cdc42. Given the low densities of GFP-Cdc42 and the inferred low plasma membrane polarity reported by Slaughter *et al.* (2013) it is difficult to reconcile their findings with our work except to note that widely different approaches were used to estimate densities.

We also demonstrate that GFP-Cdc42 is defective in its association with post-Golgi vesicles compared to its untagged counterpart. Before the work presented in this paper, common methods were limited in the ability to quantitatively examine the amounts of the native, untagged Cdc42 protein associated with post-Golgi vesicles. Thus, the inability to gather information on the native protein may have introduced gaps in our understanding that were not previously apparent. Both our data and Slaughter *et al.* [9] support the notion that Rdi1 and vesicle traffic act as parallel routes for Cdc42 cycling to and from the plasma membrane, which is somewhat surprising given the apparent recycling defect of GFP-Cdc42 compared to the untagged form [12, 25, 26]. Furthermore, it is interesting that GFP-Cdc42 supports growth of *rdi1 cdc42* cells at temperatures below 30°C (Figure 4D). This may indicate the existence of an additional or third recycling pathway that allows prenylated Cdc42 to be recycled between internal membranes and the plasma membrane polarity cap. Altogether, the data presented in this paper supports the importance of continued studies of the native protein alongside tagged forms of Cdc42 to improving our understanding of cell polarity.

## Experimental Procedures

### Yeast strains, reagents and media

Yeast strains used and generated for this study are listed in Supplemental Table S1. Standard protocols for media, growth and genetic manipulations were used. Growth media used in this study includes: YPD (1% bacto-yeast extract, 2% bacto-peptone, 2% dextrose), S minimal (0.67% yeast nitrogen base without amino acids and 2% dextrose), and dropout media (0.67% yeast nitrogen base without amino acids, synthetic complete amino acid supplement minus appropriate amino acid(s) and 2% dextrose). Media components were obtained from US Biological (Swampscott, MA), Fisher Scientific (Pittsburgh, PA) and BD

Biosciences (San Jose, CA). Galactose inductions involved growth in rich or minimal media with 3% raffinose followed by 8–10 hour inductions with 1% galactose (US Biological, Swampscott, MA). Deletion mutants were generated by PCR amplification of either a KanMX or NatMX cassette using oligos designed against the –MX cassette and flanking DNA sequences of respective genes (e.g. *END4*, *PEP12*, etc.). The genomic DNA used as PCR template was extracted from deletion strains—developed by the Saccharomyces Genome Deletion Project—using standard protocol for genomic DNA extraction [37]. Yeast transformations of the –MX cassette into *GAL*-vector, *-SRO7* and *-SEC15* strains were performed using lithium acetate method [38]. G418 sulfate was obtained from US Biological. clonNAT (nourseothricin) was obtained from WERNER BioAgents (Jena, Germany). YIpLac211-*GFP-linker-CDC42* plasmid was received as a gift from the Lew laboratory (Duke University, Durham, NC). *GFP-linker-CDC42* (behind *CDC42* promoter) was subcloned into a *LEU2*, *CEN* vector (pRS315) and introduced into wild-type and the *CDC42*-plasmid shuffle strain. Zymolyase 100T, ampicillin, Hepes (free acid), and 5-fluoroorotic acid (5-FOA) were obtained from US Biological (Swampscott, MA). Sorbitol,  $\beta$ -mercaptoethanol, phenol, sodium azide, sodium fluoride, dithiothreitol (DTT), were obtained from Sigma Aldrich (St. Louis, MO). Chloroform, Terrific Broth, and dextrose were from Fisher Scientific (Pittsburgh, PA).

### Subcellular fractionation

Wild-type and *sec6-4<sup>ts</sup>* cells with or without *PEP12* or *RDII* disruptions were grown in rich (YPD) media overnight at 25°C to mid-log phase and shifted to 37°C for 2hr to accumulate secretory vesicles. Approximately 200 OD<sub>599</sub> units of cells were harvested and washed with 10ml of (10 mM Tris pH 7.5; 20mM NaN<sub>3</sub>; 20mM NaF) buffer. Cells were spheroplasted in 7.2ml of (100 mM Tris pH 7.5; 10 mM NaN<sub>3</sub>; 1.2 M Sorbitol; 21 mM  $\beta$ -mercaptoethanol; 0.05mg/ml Zymolyase 100T) buffer for 30 min at 37°C and lysed in 6ml of ice-cold (10 mM triethanolamine, pH 7.2; 0.8M sorbitol; protease inhibitor cocktail: 2  $\mu$ g/ml each of leupeptin, aprotinin, antipain; 20  $\mu$ M pepstatin A; 2 mM 4-(2-aminoethyl)benzenesulfonyl fluoride) buffer. Lysed cells were centrifuged, cold at 450  $\times$  g for 4 min to remove unbroken cells. Cleared lysates were centrifuged in a Sorvall centrifuge (30,000  $\times$  g for 15 min at 4°C) to separate pellet and supernatant fractions. Supernatants were then centrifuged at 100,000  $\times$  g for 1hr at 4°C. Pellets were resuspended in lysis buffer at volumes equal to the supernatant fractions. Equal volumes of supernatant, pellet and total lysate fractions were boiled in SDS sample buffer and separated on a 12.5% SDS-polyacrylamide gel. Western blotting was performed using polyclonal  $\alpha$ -Sso1/2 (1:2000), polyclonal  $\alpha$ -Sec4 (1:1000) or monoclonal  $\alpha$ -Cdc42 (1:200) antibodies. Quantitative Western analysis was performed with the Odyssey Infrared Imaging System (LI-COR Biosciences, Lincoln NE).

### Plasmid shuffle assay

To determine whether *GFP-CDC42* can complement *cdc42* in GDI-depleted cells, *CDC42* (*CEN*, *HIS*) or *GFP-linker-CDC42* (*CEN*, *HIS*) were transformed into *CDC42* plasmid shuffle strains that were either wild-type or disrupted for *RDII*. Deletion of *RDII* was accomplished by homologous recombination as described for the endocytic deletion mutants. After selection on sc-his plates, the original *CDC42* plasmid (*CEN*, *URA*) was

evicted by growth on 5-FOA. Temperature sensitivity was evaluated at temperatures ranging from 14°C to 37.5°C. Images of higher temperatures shown in Figure 4 represent phenotypic separation between the *RDII* and *rdiI* strains.

### Immunofluorescence and fluorescence microscopy

Cells were grown to mid-log phase in 2% glucose media and shifted into 3% raffinose for 2/+ doublings. *GAL-SRO7* and *-SEC15* were induced by adding 1% galactose for 8–10 hours. Cells were fixed and processed for immunofluorescent staining as described previously [31, 39]. Double-labeled immunofluorescent staining of the plasma membrane polarity cap and post-Golgi vesicles was performed using ammonium sulfate precipitated, monoclonal mouse  $\alpha$ -Sec4 (1:200) and affinity-purified, polyclonal rabbit  $\alpha$ -Cdc42 (1:75) antibodies. For background correction, control staining was performed using rabbit and mouse IgG antibodies that lacked reactivity to any yeast protein. Secondary antibodies were Rhodamine Red-X-conjugated AffiniPure Goat Anti-Mouse IgG and Fluorescein Isothiocyanate (FITC)-conjugated AffiniPure Goat Anti-Rabbit IgG (Jackson ImmunoResearch Laboratories Inc., West Grove, PA), respectively. Secondary antibodies were used at 1:100–1:200 dilution. Single-plane immunofluorescent, GFP-fluorescent, and differential interference contrast (DIC) images were acquired using Nikon model E600 and 2D-deconvolved using MetaMorph software (Molecular Devices). Figures were prepared from deconvolved images using Adobe Photoshop and Illustrator (CS5.1).

### Quantitative analysis of polarized and vesicle clustering cells

ImageJ [40] was used to conduct quantitative analysis of single plane, 2D-deconvolved images. Cdc42 fluorescence intensity (a.u.) was measured using regions of interest (ROIs) drawn within the centroid, or peak intensity, of either the plasma membrane polarity cap or the post-Golgi vesicle cluster and throughout the cytoplasm of the respective cell. Increases in fluorescence intensities of Cdc42 associated with the polarity cap versus the cluster relative to the cytoplasm were calculated in Microsoft Excel. Data was presented as either 1) relative fluorescence: the ratio of the average fluorescence intensities of the Cdc42-positive compartment relative to the cytosol, 2) relative association: the Cdc42 compartment:cytosol ratio expressed as percent association relative to 100% wild-type, 3) phenotype penetrance: box and whisker plot of the Cdc42 compartment:cytosol ratio. Figures were prepared using Adobe Photoshop and Illustrator (CS5.1).

### Ratio-metric analysis of GFP-Cdc42 using the Cse4 reference standard

Cells expressing either GFP-Cdc42 or Cse4-GFP were cultured at 25°C in minimal media to mid-log phase. Equivalent OD<sub>599</sub> of both strains were mixed and spread onto standard, uncoated microscope slides. Images were acquired as 400ms/frame, 24-frame Z-series, with 0.2 $\mu$ m step-size using an Olympus IX81 microscope. Additionally, cells were imaged using differential interference contrast alongside fluorescence acquisition to delineate cells. Image 3D deconvolution was performed using MetaMorph software (version 7.7.10.0; Molecular Devices) and sum-intensity projections and measurements using ImageJ [40]. Integrated fluorescence intensity and background correction for Cse4-GFP was obtained as described in Lawrimore *et al.* [30]. ROIs were drawn around the periphery of incipient and small-

budded cells to obtain the total cellular integrated fluorescence intensity for GFP-Cdc42. Background corrections were obtained from whole cell ROIs of controls cells that were imaged in mixture with GFP-Cdc42 expressing cells. Total copies of GFP-Cdc42 in the cell were calculated by: (average GFP-Cdc42 fluorescence intensity  $\div$  average Cse4-GFP fluorescence intensity)  $\times$  80 Cse4-GFP copies/cell (yielded  $\sim$ 27,400 copies/cell). Approximately 40 cells for each strain were measured.

### Comparative analysis of Cdc42 protein

To compare the amounts of endogenous Cdc42 to the plasmid-derived tagged and untagged forms, quantitative Western analysis was performed using the Odyssey Infrared Imaging System (LI-COR Biosciences, Lincoln NE). Strains were grown overnight (25°C) in minimal media to mid-log phase. Cells were then transferred to rich media for 2 doublings prior to harvesting 7 OD<sub>599</sub> units for glass bead lysis. An aliquot of each of these cultures were diluted to 0.2–0.4 OD<sub>599</sub> units and counted using a hemocytometer. Cells were then subjected to glass bead lysis and lysates boiled in SDS sample buffer. Lysates were normalized based on equivalent cell number, separated on an 11.5% polyacrylamide gel and analyzed by quantitative western blotting. The ratio of protein amounts of GFP-tagged to endogenous Cdc42 were applied to the total cellular copies of GFP-Cdc42 to determine the total cellular copies of the native, untagged protein (yielded  $\sim$ 6,800 copies/cell).

Quantitative Western blotting was also used to compare Cdc42 amounts in wild-type and vesicle clustering strains. Cells were cultured using the same growth conditions as for fluorescence imaging and loaded on a polyacrylamide gel based on equivalent cell number. The ratio of protein amounts of wild-type and vesicle clustering strains yielded  $\sim$ 10,400 copies of Cdc42 in *GAL-SEC15* induced cells.

### Ratio-metric analysis of GFP-Cdc42 using the Sec1 reference standard

To generate the reference standard strain, an EcoR1 linearized plasmid (pB1114) containing a N-terminal deletion of *SEC1* tagged with GFP was integrated into wild-type cells at the *SEC1* locus using standard yeast transformation method [38]. The resulting strain expresses *SEC1-GFP* as the sole copy in the cell. Cells expressing either GFP-Cdc42 or Sec1-GFP, as the sole source, were cultured and prepared for quantitative Western blotting as described for comparative analysis of Cdc42 protein (above). Western blotting was performed using monoclonal mouse  $\alpha$ -GFP from Roche Diagnostics (Indianapolis, IN), polyclonal rabbit  $\alpha$ -Adh1 (1:2000), or affinity purified polyclonal  $\alpha$ -Exo70 (1:100) antibodies. The total copies of Sec1 per cell [27] was applied to the ratio of GFP-Cdc42:Sec1-GFP to obtain total cellular copies of GFP-Cdc42 ( $\sim$ 21,500 copies/cell). The comparative analysis of plasmid-borne to native Cdc42, induced to uninduced cells was applied to determine the total native Cdc42 copies per cell in uninduced and induced cells,  $\sim$ 5,400 and 8,200 respectively.

### Quantification of Cdc42 vesicle and polarity cap surface densities

*GAL*-induced vesicle clustering strains and the vector control strain were cultured and processed for immunofluorescence as previously described. Image acquisition for fixed samples was as follows: 800ms/frame, 14 to 18-frame Z-series, with 0.2 $\mu$ m step-size using an Olympus IX81 microscope. Image 3D deconvolution, sum-intensity projections and ROI

measurements were performed to obtain the integrated fluorescence of the entire cell (as described for GFP-Cdc42). Also from these deconvolved z-series, ROI scans for the polarity cap and vesicle cluster were performed on the z-plane with the peak Cdc42 integrated fluorescence signal. ROI diameters used for polarity cap (0.47 $\mu\text{m}$ ) and vesicle cluster (0.72 $\mu\text{m}$ ) were chosen based on size that consistently fit regions with homogeneous staining. The fractional amount of the total integrated fluorescence intensity for the polarity cap and cluster was determined and converted to copies per ROI using this work's estimates of the total copies of the native protein per cell. Approximately 50 cells per strain were used for this analysis.

Morphometric analysis of thin-section micrographs was performed to obtain surface densities of the polarity cap and vesicle cluster. Vesicle cluster analysis: vesicles were counted in six regions of known size in several thin-section micrographs yielding an average cluster packing density of  $35.5 \pm 3.9$  vesicles/ $\mu\text{m}^2$ . A 0.2 $\mu\text{m}$ -thick z-plane can accommodate two vesicles with a 90nm diameter. With this two-vesicle maximum per optical section and an ROI area of 0.407 $\mu\text{m}^2$ , we estimate that each ROI used for immunofluorescence contains an average of 71 vesicles/ROI and a total vesicle membrane surface area of 0.72 $\mu\text{m}^2$ . Polarity cap analysis: small-budded wild-type cells from six independent EM fields were examined for the absence/presence of vesicles within the bud that were either associated with or adjacent to the plasma membrane. This analysis yielded an average of  $1.3 \pm 0.23$  vesicles/ $\mu\text{m}^2$  per thin-section or 2.6 vesicles/ $\mu\text{m}^2$  per IF optical section. The resulting surface density was subtracted from the final polarity cap density and the average copies per ROI, surface area and density for the polarity cap are reported alongside those for the vesicle cluster in Figure 5.

## Supplementary Material

Refer to Web version on PubMed Central for supplementary material.

## Acknowledgements

We thank Tim Elston, Danny Lew and Kerry Bloom for reagents and helpful discussions, Tim Elston and Ken Jacobson for access to the spinning disk microscope, Doug Cyr and Robert Currin for imaging software usage, Josh Kelley, Gauri Dixit, Michelle Itano, and Katie Wolfe for assistance with fluorescence imaging, Chavela Carr for *SECI-GFP* plasmid, and Kelly Watson for comments on the manuscript. This work was supported by grants to PB (GM054712) and LJW (IMSD T32GM055336; CMB T32GM008581; F31GM096734).

## References

1. Ziman M, Preuss D, Mulholland J, O'Brien JM, Botstein D, Johnson DI. Subcellular localization of Cdc42p, a *Saccharomyces cerevisiae* GTP-binding protein involved in the control of cell polarity. *Mol Biol Cell*. 1993; 4:1307–1316. [PubMed: 8167411]
2. Slaughter BD, Smith SE, Li R. Symmetry breaking in the life cycle of the budding yeast. *Cold Spring Harb Perspect Biol*. 2009; 1:a003384. [PubMed: 20066112]
3. Wu H, Brennwald P. The function of two Rho family GTPases is determined by distinct patterns of cell surface localization. *Mol Cell Biol*. 2010; 30:5207–5217. [PubMed: 20823269]
4. Howell AS, Lew DJ. Morphogenesis and the cell cycle. *Genetics*. 2012; 190:51–77. [PubMed: 22219508]
5. Johnson DI. Cdc42: An essential Rho-type GTPase controlling eukaryotic cell polarity. *Microbiol Mol Biol Rev*. 1999; 63:54–105. [PubMed: 10066831]

6. Bi E, Park HO. Cell polarization and cytokinesis in budding yeast. *Genetics*. 2012; 191:347–387. [PubMed: 22701052]
7. Wedlich-Soldner R, Wai SC, Schmidt T, Li R. Robust cell polarity is a dynamic state established by coupling transport and GTPase signaling. *J Cell Biol*. 2004; 166:889–900. [PubMed: 15353546]
8. Irazoqui JE, Howell AS, Theesfeld CL, Lew DJ. Opposing roles for actin in Cdc42p polarization. *Mol Biol Cell*. 2005; 16:1296–1304. [PubMed: 15616194]
9. Slaughter BD, Das A, Schwartz JW, Rubinstein B, Li R. Dual modes of Cdc42 recycling fine-tune polarized morphogenesis. *Dev Cell*. 2009; 17:823–835. [PubMed: 20059952]
10. Ozbudak EM, Becskei A, van Oudenaarden A. A system of counteracting feedback loops regulates Cdc42p activity during spontaneous cell polarization. *Dev Cell*. 2005; 9:565–571. [PubMed: 16198298]
11. Orlando K, Sun X, Zhang J, Lu T, Yokomizo L, Wang P, Guo W. Exo-endocytic trafficking and the septin-based diffusion barrier are required for the maintenance of Cdc42p polarization during budding yeast asymmetric growth. *Mol Biol Cell*. 2011; 22:624–633. [PubMed: 21209323]
12. Freisinger T, Klunder B, Johnson J, Muller N, Pichler G, Beck G, Costanzo M, Boone C, Cerione RA, Frey E, Wedlich-Soldner R. Establishment of a robust single axis of cell polarity by coupling multiple positive feedback loops. *Nat Commun*. 2013; 4:1807. [PubMed: 23651995]
13. Jose M, Tollis S, Nair D, Sibarita JB, McCusker D. Robust polarity establishment occurs via an endocytosis-based cortical corralling mechanism. *J Cell Biol*. 2013; 200:407–418. [PubMed: 23401000]
14. Wedlich-Soldner R, Altschuler S, Wu L, Li R. Spontaneous cell polarization through actomyosin-based delivery of the Cdc42 GTPase. *Science*. 2003; 299:1231–1235. [PubMed: 12560471]
15. Forsmark A, Rossi G, Wadskog I, Brennwald P, Warringer J, Adler L. Quantitative proteomics of yeast post-Golgi vesicles reveals a discriminating role for Sro7p in protein secretion. *Traffic*. 2011; 12:740–753. [PubMed: 21477180]
16. Layton AT, Savage NS, Howell AS, Carroll SY, Drubin DG, Lew DJ. Modeling vesicle traffic reveals unexpected consequences for Cdc42p-mediated polarity establishment. *Curr Biol*. 2011; 21:184–194. [PubMed: 21277209]
17. Salminen A, Novick PJ. The Sec15 protein responds to the function of the GTP binding protein, Sec4, to control vesicular traffic in yeast. *J Cell Biol*. 1989; 109:1023–1036. [PubMed: 2504727]
18. Rossi G, Brennwald P. Yeast homologues of lethal giant larvae and type V myosin cooperate in the regulation of Rab-dependent vesicle clustering and polarized exocytosis. *Mol Biol Cell*. 2011; 22:842–857. [PubMed: 21248204]
19. Guo W, Roth D, Walch-Solimena C, Novick P. The exocyst is an effector for Sec4p, targeting secretory vesicles to sites of exocytosis. *EMBO J*. 1999; 18:1071–1080. [PubMed: 10022848]
20. Pfeffer SR, Dirac-Svejstrup AB, Soldati T. Rab GDP dissociation inhibitor: putting rab GTPases in the right place. *J Biol Chem*. 1995; 270:17057–17059. [PubMed: 7615494]
21. Yamamoto T, Mochida J, Kadota J, Takeda M, Bi E, Tanaka K. Initial polarized bud growth by endocytic recycling in the absence of actin cable-dependent vesicle transport in yeast. *Mol Biol Cell*. 2010; 21:1237–1252. [PubMed: 20147449]
22. Raths S, Rohrer J, Crausaz F, Riezman H. end3 and end4: two mutants defective in receptor-mediated and fluid-phase endocytosis in *Saccharomyces cerevisiae*. *J Cell Biol*. 1993; 120:55–65. [PubMed: 8380177]
23. Boulter E, Garcia-Mata R, Guilluy C, Dubash A, Rossi G, Brennwald PJ, Burridge K. Regulation of Rho GTPase crosstalk, degradation and activity by RhoGDI1. *Nat Cell Biol*. 2010; 12:477–483. [PubMed: 20400958]
24. Shaw JD, Cummings KB, Huyer G, Michaelis S, Wendland B. Yeast as a model system for studying endocytosis. *Exp Cell Res*. 2001; 271:1–9. [PubMed: 11697876]
25. Bi E, Chiavetta JB, Chen H, Chen GC, Chan CS, Pringle JR. Identification of novel, evolutionarily conserved Cdc42p-interacting proteins and of redundant pathways linking Cdc24p and Cdc42p to actin polarization in yeast. *Mol Biol Cell*. 2000; 11:773–793. [PubMed: 10679030]
26. Howell AS, Jin M, Wu CF, Zyla TR, Elston TC, Lew DJ. Negative feedback enhances robustness in the yeast polarity establishment circuit. *Cell*. 2012; 149:322–333. [PubMed: 22500799]

27. Ghaemmaghami S, Huh WK, Bower K, Howson RW, Belle A, Dephoure N, O'Shea EK, Weissman JS. Global analysis of protein expression in yeast. *Nature*. 2003; 425:737–741. [PubMed: 14562106]
28. Joglekar AP, Bouck DC, Molk JN, Bloom KS, Salmon ED. Molecular architecture of a kinetochore-microtubule attachment site. *Nat Cell Biol*. 2006; 8:581–585. [PubMed: 16715078]
29. Joglekar AP, Salmon ED, Bloom KS. Counting kinetochore protein numbers in budding yeast using genetically encoded fluorescent proteins. *Methods Cell Biol*. 2008; 85:127–151. [PubMed: 18155462]
30. Lawrimore J, Bloom KS, Salmon ED. Point centromeres contain more than a single centromere-specific Cse4 (CENP-A) nucleosome. *J Cell Biol*. 2011; 195:573–582. [PubMed: 22084307]
31. Roumanie O, Wu H, Molk JN, Rossi G, Bloom K, Brennwald P. Rho GTPase regulation of exocytosis in yeast is independent of GTP hydrolysis and polarization of the exocyst complex. *J Cell Biol*. 2005; 170:583–594. [PubMed: 16103227]
32. Wu H, Rossi G, Brennwald P. The ghost in the machine: small GTPases as spatial regulators of exocytosis. *Trends Cell Biol*. 2008; 18:397–404. [PubMed: 18706813]
33. Savage NS, Layton AT, Lew DJ. Mechanistic mathematical model of polarity in yeast. *Mol Biol Cell*. 2012; 23:1998–2013. [PubMed: 22438587]
34. Okada S, Leda M, Hanna J, Savage NS, Bi E, Goryachev AB. Daughter cell identity emerges from the interplay of Cdc42, septins, and exocytosis. *Dev Cell*. 2013; 26:148–161. [PubMed: 23906065]
35. Dyer JM, Savage NS, Jin M, Zyla TR, Elston TC, Lew DJ. Tracking shallow chemical gradients by actin-driven wandering of the polarization site. *Curr Biol*. 2013; 23:32–41. [PubMed: 23200992]
36. Slaughter BD, Unruh JR, Das A, Smith SE, Rubinstein B, Li R. Non-uniform membrane diffusion enables steady-state cell polarization via vesicular trafficking. *Nat Commun*. 2013; 4:1380. [PubMed: 23340420]
37. Hoffman CS. Preparation of yeast DNA. *Curr Protoc Mol Biol*. 2001; Chapter 13(Unit13):1.
38. Moerschell, RP.; Das, G.; Sherman, F. Christine Guthrie GRF. *Methods in Enzymology*. Vol. 194. Academic Press; 1991. [24] Transformation of yeast directly with synthetic oligonucleotides; p. 362-369.
39. Brennwald P, Novick P. Interactions of three domains distinguishing the Ras-related GTP-binding proteins Ypt1 and Sec4. *Nature*. 1993; 362:560–563. [PubMed: 8464498]
40. Schneider CA, Rasband WS, Eliceiri KW. NIH Image to ImageJ: 25 years of image analysis. *Nat Methods*. 9:671–675. [PubMed: 22930834]

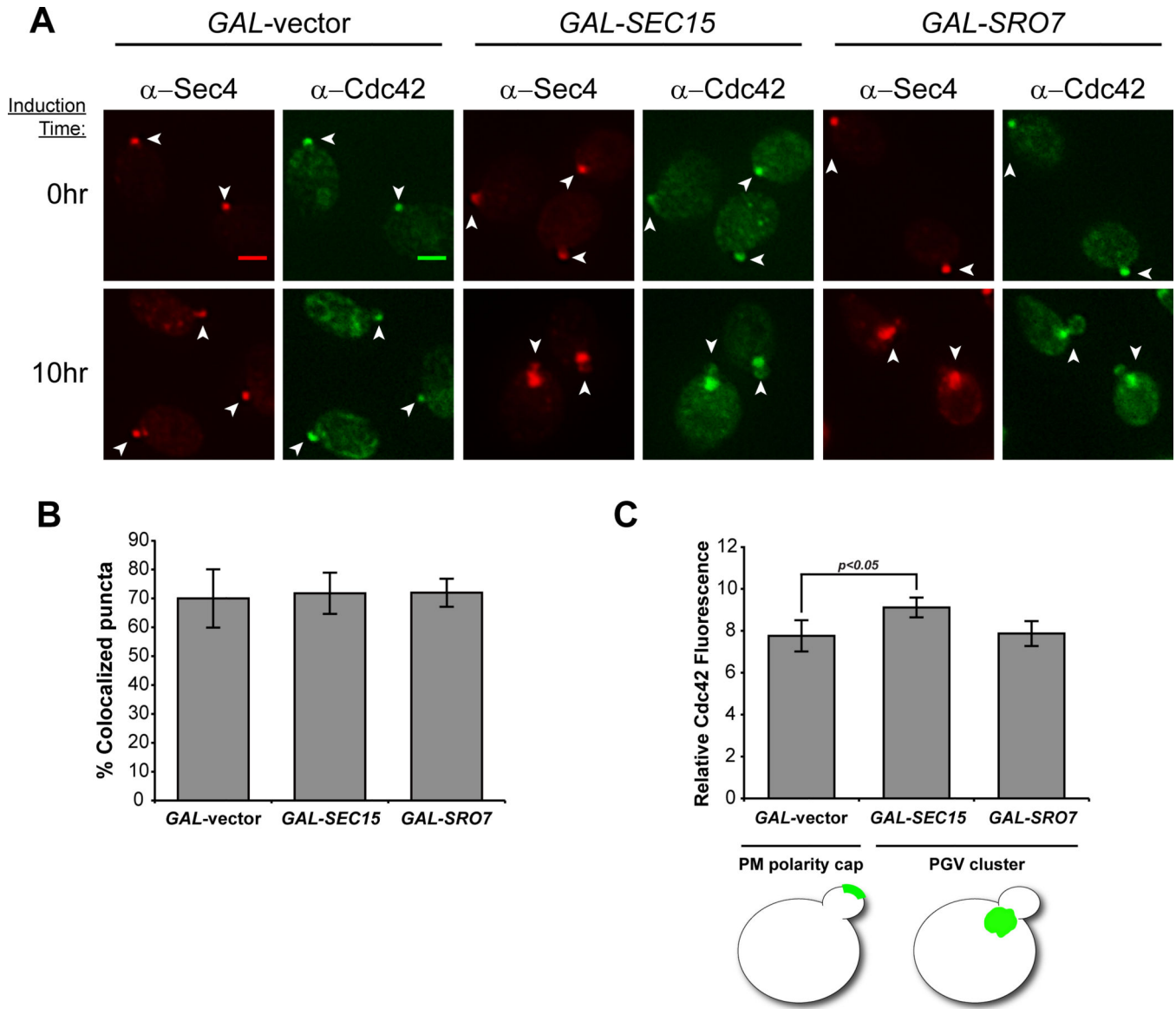


**Figure 1. An *in vivo* assay demonstrates the association of Cdc42 with post-Golgi vesicles**  
**A)** Cdc42 localizes to Sec4+ post-Golgi vesicle clusters following *GAL*-overexpression of *Sro7* and *Sec15*. Induced and uninduced cells were subjected to fixation and double-label immunofluorescence using monoclonal  $\alpha$ -mouse Sec4 (red) and polyclonal  $\alpha$ -rabbit Cdc42 (green) antibodies. Single-plane, 2D deconvolved images are shown. Cdc42/Sec4 co-staining for the plasma membrane polarity cap and post-Golgi vesicle clusters is denoted by arrowheads. Scale bar = 2 $\mu$ m. **B & C)** Quantitative analyses of Cdc42 association with Sec4+ compartments. **B)** Approximately 40 cells were selected based on Sec4+ staining and scored for Cdc42 co-localization. The bar graph compares the percentage of puncta showing co-localization in polarized and cluster-forming cells. Error bars represent standard deviation. **C)** The average ratio of Cdc42 at the polarity cap or vesicle clusters over the cytoplasm was measured (see Experimental Procedures) in cells acquired from three independent experiments (approx. 140 cells). Error bars represent the standard deviation.

Two-tailed Student  $t$  test was performed comparing vesicle clusters to the polarity cap (vector control).  $p=0.022$

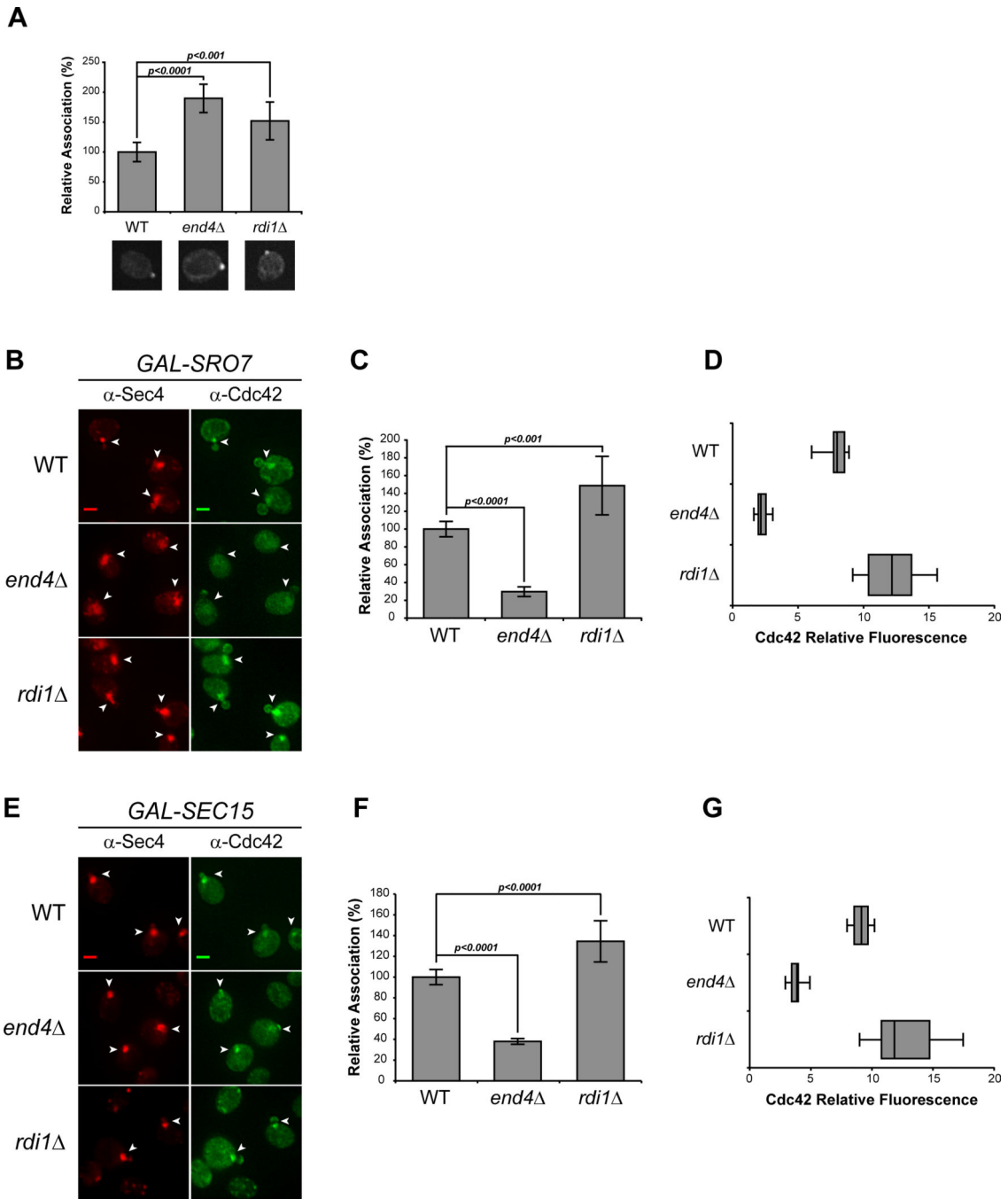


**Figure 2. Endocytosis, but not Rho GDI, is required for Cdc42 association with post-Golgi vesicles**

**A**) Cdc42 associates with the plasma membrane polarity cap in *RDII*- and *END4* (*SLA2*)-depleted cells. Deletions in *RDII* and *END4* were introduced into the *GAL-SRO7* vesicle clustering strain (see Experimental Procedures). Cells were grown in raffinose media (25°C) and subjected to IF as in Figure 1. The percent association of Cdc42 at the plasma membrane polarity cap in uninduced wild-type, *rdi1* and *end4* cells were compared. Single-cell images represent the mean relative association; approx. 40 cells were scored;

error bars represent the standard deviation. Two-tailed Student *t* test was performed to compare mutants to WT. **B–G**) Endocytic block impedes Cdc42 vesicle association. **B & E**) Galactose induction of vesicle clusters and IF staining was performed on wild-type, *rdi1*, and *end4* cells as described in Figure 1. Vesicle clusters are denoted by arrowheads. Scale bar = 2 $\mu$ m. **C & F**) Quantitative representation of the association of Cdc42 with Sro7- and Sec15-induced vesicle clusters (B & E respectively). The average Cdc42 fluorescence intensity was measured in cells randomly selected for Sec4+ vesicle clusters. Approximately 100 cells for each strain were scored. Error bars represent standard deviation. Data were normalized to percent association relative to 100% associated wild-type. Two-tailed Student *t* test was used to compare mutants to wild-type. **D & G**) Penetrance of *end4* phenotype is shown as a box-and-whisker plot. The box represents the interquartile range (IQR) of the average relative Cdc42 fluorescence intensity. The line and whiskers denote the median and minimum/maximum, respectively.

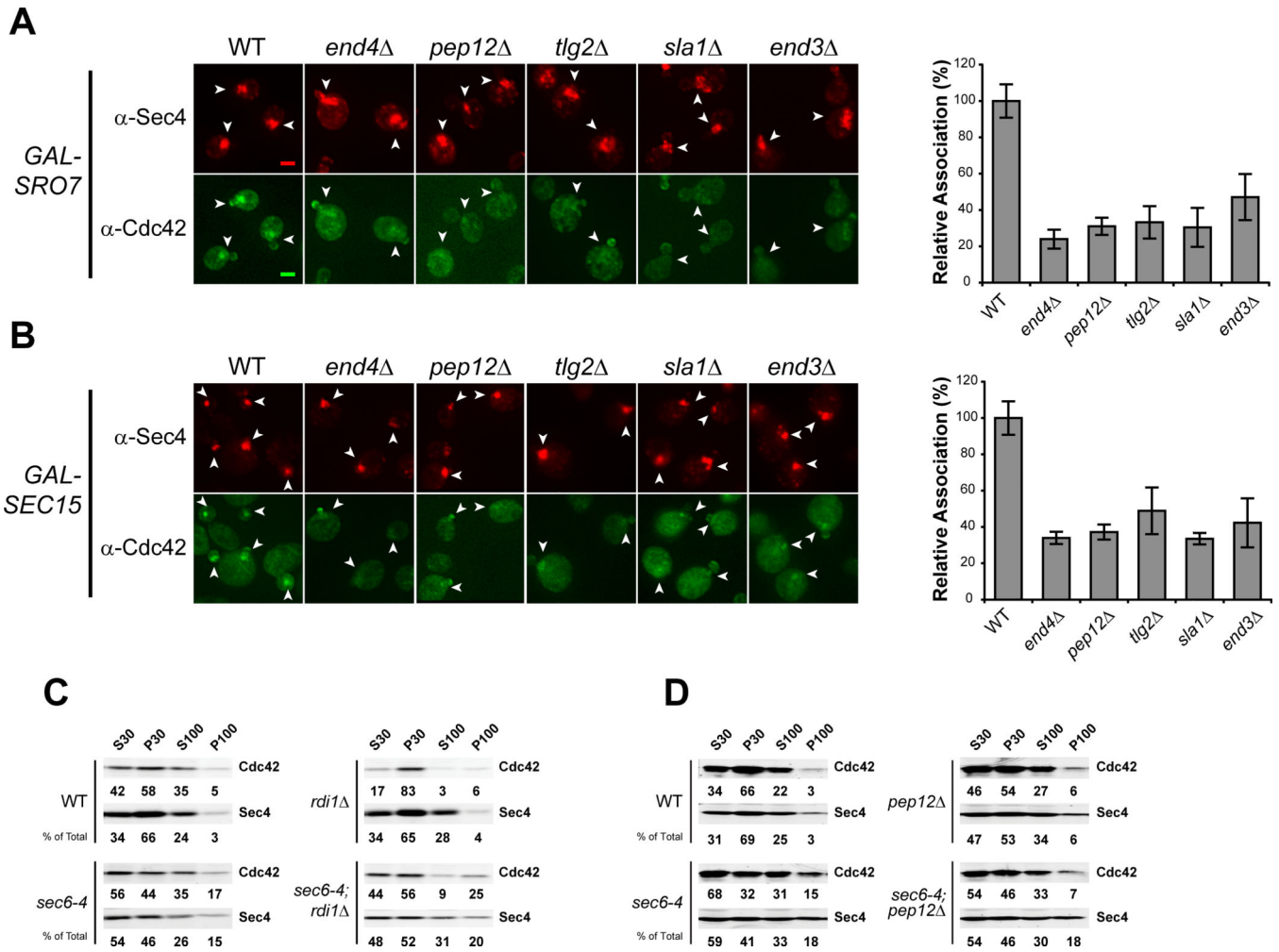


**Figure 3. Endosomal sorting mutants show defects in Cdc42 recycling onto post-Golgi vesicles**  
**A & B)** Deletions in general endocytic regulators were introduced into the *GAL-SRO7* and *SEC15* strains (see Experimental Procedures). Cells were induced, fixed and subjected to IF as in Figure 2. Effect on Cdc42 vesicle cluster association is denoted by arrowheads. Data is presented as percent association relative to wild-type. Approximately 40 cells per strain were scored. Student *t* test was performed on all endocytic mutants compared to wild-type: A & B): all comparisons yielded  $p < 0.0001$ . Scale bar = 2μm. **C & D)** Cdc42 associates with *sec6-4* derived post-Golgi vesicles in an endocytic-dependent, *RDII*-independent manner. *PEP12* and *RDII* disruptions were introduced into the late-secretory mutant *sec6-4* and an isogenic wild-type strain. Strains were grown in rich media overnight at 25°C to mid-log phase and shifted to 37°C for 2h to accumulate secretory vesicles. Cells were lysed and differential centrifugation was performed. Samples of low- and high-speed supernatants (S30 and S100) and pellets (P30 and P100) fractions were subjected to SDS-PAGE and Western analyses using antibodies against Sec4 and Cdc42 (see Experimental Procedures). Percentages of total protein are shown under each blot.

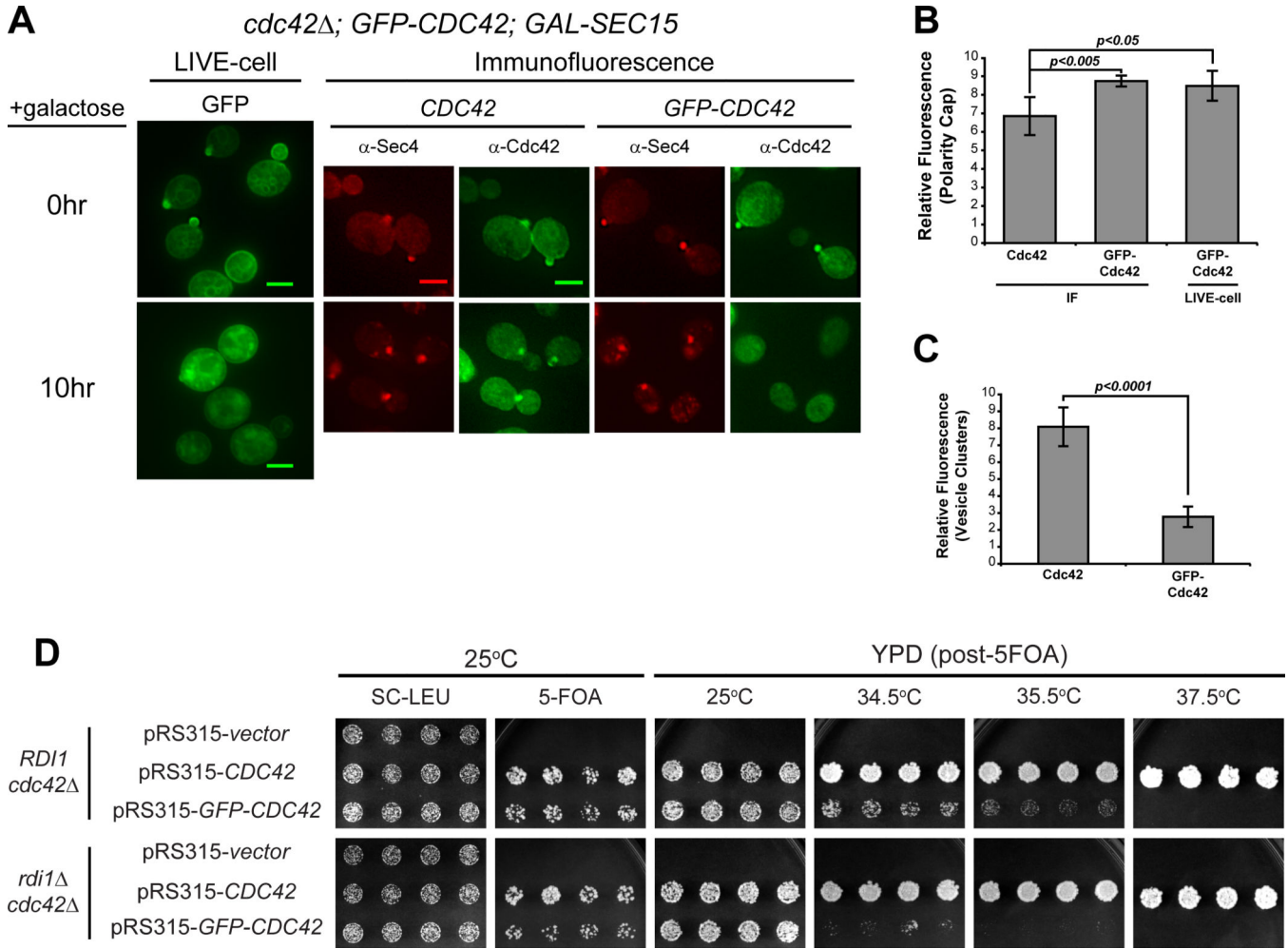


**Figure 4. GFP-tagged Cdc42 has impaired ability to associate with post-Golgi vesicles and exhibits synthetic growth defects with *rdi1***

**A)** GFP-Cdc42 does not accumulate under conditions that form Sec4+ post-Golgi vesicle clusters. Vesicles clusters were induced in cells that complement a *cdc42* with either untagged or GFP-tagged *CDC42* expressed behind the *CDC42* promoter on a *LEU2/CEN* plasmid. Cdc42 vesicle and PM association was visualized by double-labeled IF of Sec4 and Cdc42. Live cell imaging of GFP-Cdc42 was performed before and after *GAL*-induction. **B & C)** Quantitative analysis of average relative GFP-Cdc42 fluorescence intensity at the PM (B, live-cell versus IF) and the cluster (C, IF only). Polarity cap (B):  $n = 25$ . Vesicle cluster (C):  $n = 50$ . Data comparing GFP-Cdc42 expressing cells to untagged Cdc42 (*CEN*) was analyzed by Student *t* test. (B) Comparison of Live, GFP-Cdc42 to native Cdc42 by IF:  $p=0.0235$  Scale bar =  $4\mu\text{m}$  **D)** *GFP-CDC42* is synthetically sick with *rdi1*. Untagged or GFP-tagged *CDC42* were introduced into *CDC42*-plasmid shuffle strains that contained either *RDI1* or *rdi1*. After selection on 5-FOA, growth on YPD was assessed at 25°C, 34.5°C, 35.5°C and 37.5°C.

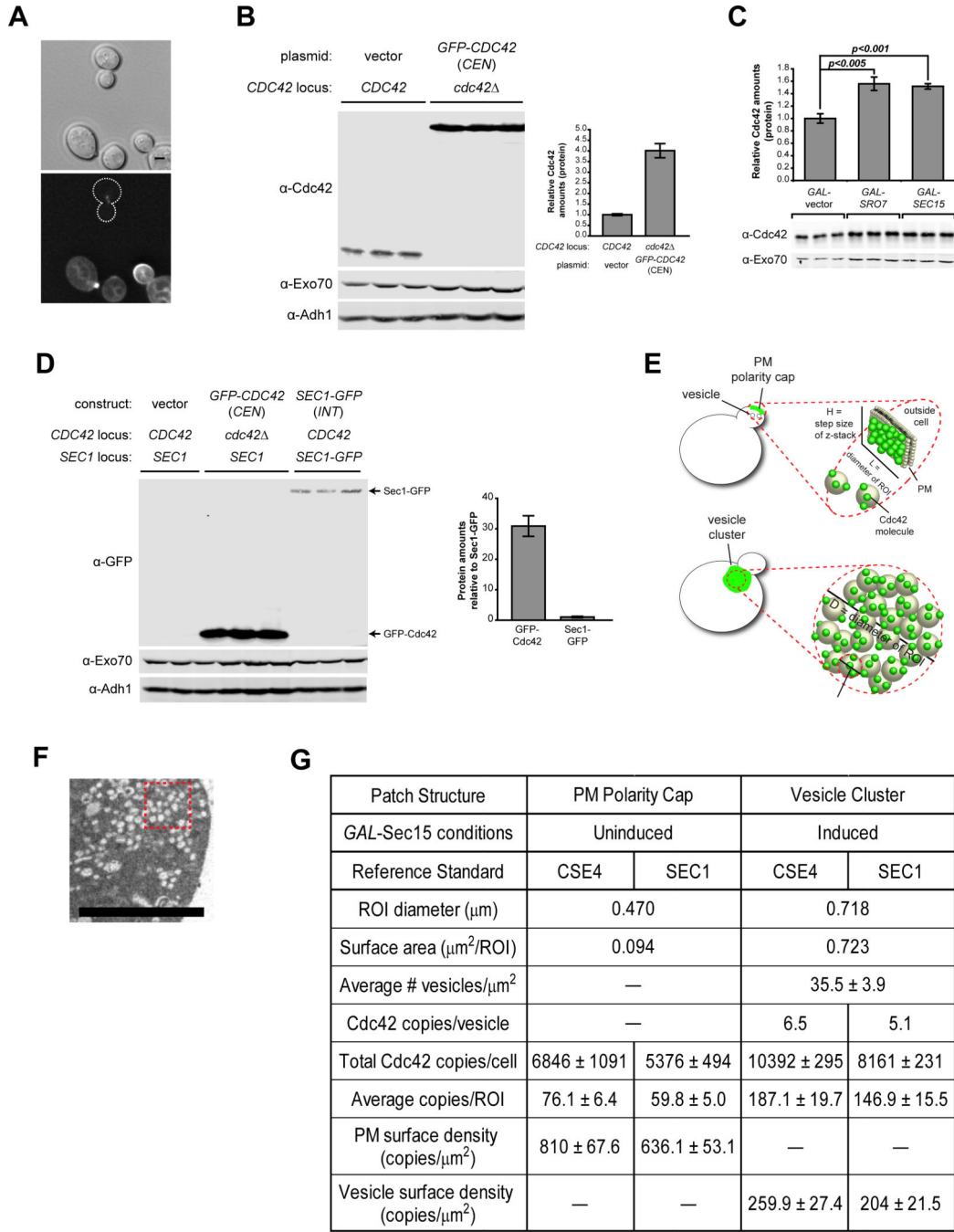


**Figure 5. Quantitative analysis of Cdc42 density on post-Golgi vesicles and the plasma membrane polarity cap**

**A)** Fluorescence signal differences in GFP-Cdc42 and the reference standard, Cse4-GFP. Micrographs shown are sum-intensity projections from 24 deconvolved z-planes (bottom) and the reference differential interference contrast (top). Scale bar = 2 $\mu\text{m}$ . **B)** Whole cell lysate comparison of cells expressing GFP-Cdc42 (*CEN*) or the chromosomal (untagged) Cdc42 in rich media. Protein samples were normalized by cell equivalents as described in Experimental Procedures. Antibodies against Exo70 and Adh1 were used as loading

controls. Quantification of the relative Cdc42 protein levels in GFP-Cdc42 expressing cells compared to cells expressing chromosomal Cdc42—when normalized by equivalent cell number. **C)** Whole cell lysate comparison of Cdc42 protein levels in vector, *GAL-Sro7* and *Sec15* after 8h induction in 1% galactose. Protein samples were loaded in duplicate based on equivalent cellular number. *Exo70* was used as a loading control. Student *t* test was performed to compare relative Cdc42 amounts in clustering (*GAL-Sro7* or *-Sec15*) versus non-clustering wild-type cells (vector). **D)** Whole cell lysate comparison of GFP-tagged Cdc42 (*CEN*) and *Sec1-GFP (INT)* in rich media. Protein samples were loaded in triplicate based on equivalent cell number. Western blotting was performed using monoclonal  $\alpha$ -GFP and polyclonal  $\alpha$ -*Exo70* and  $\alpha$ -*Adh1* antibodies. Quantification of amounts of GFP-tagged protein relative to *Sec1-GFP* are shown. **E)** Schematic representation of measured surface densities associated with the polarity cap and vesicle cluster. **F)** Representative thin-section electron micrograph of vesicle cluster packing density. The thickness of each optical sections is 60nm. Scale bar = 2 $\mu$ m. **G)** Table of Cdc42 density estimates in polarity cap and vesicle cluster using *Cse4* or *Sec1* reference standards.